*Journal of Sound and Vibration* (1998) **212**(2), 275–294

# A VARIATIONAL APPROACH FOR THE STUDY OF OUTDOOR SOUND PROPAGATION AND APPLICATION TO RAILWAY NOISE

P. JEAN

*Centre Scientifique et Technique du Bâtiment*, 24 *rue Joseph Fourier*, 38400 *Saint-Martin-d'Hères*, *France*.

(*Received* 30 *June* 1997, *and in final form* 19 *November* 1997)

A boundary element program for the study of 2D acoustical problems is presented. It uses a variational approach leading to symmetric matrices after discretization. Numerical optimization enables the study of complex situations, such as screens placed near trains, for the full frequency range of interest, at reasonable cost. The ground effect is included in the Green function. Post-treatments offer means of introducing point or incoherent line sources. Several applications to the cases of screens placed near trains are given.



## 1. INTRODUCTION

The study of outdoor sound propagation may involve different levels of complexity such as long distance effects, complex obstacles eventually absorbent, meteorological effects. Geometrical approaches may deal with complex ground profiles and multiple reflections provided that no close effects prevail. Simple formulae [1] such as the now classical Maekawa model have proved efficient for straight screens. The geometrical theory of diffraction [2] can deal with more complex situations but will fail, for instance, to predict the effect of an absorbent material placed on top of a T-shaped screen. Complex ground profiles may be introduced. Meteorological effects have been studied with various approaches, as for instance with the parabolic equation method [3].

So various methods may be used depending on the problem. If the main concern is the optimization of noise barriers, precise results are required and finite element techniques are well known for their accuracy provided that one is ready to pay for the usually high computation times and that one is interested only in the low frequencies. The boundary element method (BEM) appears well suited for outdoor sound propagation since it leads to the discretization of surfaces only, and includes the conditions of sound radiation at infinity. Furthermore, if the ground is assumed infinite, flat and of constant admittance, its discretization can be avoided, provided that the elementary solution includes the reflection by the ground [4].

In this paper, a boundary element formalism is presented [5–8]. A variational approach is used which leads to symmetric matrices after discretization. The developments are made for 2D situations, which offer the great advantage of permitting the study of the full audio frequency range. Recent works by Duhamel [10, 11] extended the method to 3D situations where the geometry remains infinite along one dimension but with the possibility of including point or infinite incoherent line sources which are closer to real traffic sources. Several applications are reported for different shapes of screens, alone or in the near field

0022–460X/98/170275 + 20 $25.00/0/sv971407 

of trains. 3D applications are presented and the efficiencies of screens are compared for infinite line sources, either coherent or incoherent.

## 2. THE INTEGRAL REPRESENTATION

Figure 1 shows the geometry of the problem which remains constant along the $y$-axis. The analysis is done for the harmonic time dependence $e^{-i\omega t}$. $E$ is an infinite coherent line source which therefore appears as a point source in the 2D representation. The ground $L$, along $x$, is flat, of infinite extent, and may be either rigid or of constant admittance $\alpha$. $A$ and $B$ are contours having an admittance $Y$ different from $\alpha$, $A$ being on the ground. $A$ and $B$ may be of variable admittance with position, $n$ is the normal to the boundaries, directed towards the fluid. The admittances are defined as ratios of displacement to pressure, rather than velocity to pressure, thus avoiding i terms in the integral representations.

The Green integral can be expressed as

$$P(M) = \int_S P(Q)[\rho\omega^2 Y(Q)G(M, Q) - \partial G(M, Q)/\partial n_Q]\,\mathrm{d}S(Q) + t(M), \tag{1}$$

where $P(M)$ is the acoustical pressure at any point $M$ outside $L \cup S$ ($S = A \cup B$). $G(M, Q)$ is the Green solution of the problem and it gives the elementary solution at any point $M$ when only the ground $L$ is present in the case of a unit line source at any point $Q$. $S_0$ is the position of the line source, $t(M)$ is the solution when only $L$ is present, and $\rho$ is the fluid density.

The integral gives the total pressure radiated by the screen ($A$ and $B$ surfaces).

The expression for $G$ is the sum of three terms [8]:

$$G(M, Q) = -(\mathrm{i}/4)\mathrm{H}_0(kr) - (\mathrm{i}/4)\mathrm{H}_0(kr^-) + P_\alpha(M, Q), \tag{2}$$

where $r$ is the $(M, Q)$ distance, $r^-$ is the distance between $M$ and the image of $Q$ with respect to $L$, and $\mathrm{H}_0$ is the Hankel function of the first kind and order zero. The second term is the contribution of a hard floor, and $P_\alpha$ is the correction factor for ground admittance:

$$P_\alpha(M, Q) = \frac{\mathrm{i}\beta}{2\pi}\int_{-\infty}^{\infty} \frac{\exp\left(\mathrm{i}k[(y_M + y_Q)(1 - s^2)^{1/2} - (x_M - x_Q)s]\right)}{(1 - s^2)^{1/2}[(1 - s^2) + \beta]}\,\mathrm{d}s, \qquad \mathrm{Re}\,\beta > 0. \tag{3}$$

Here $\beta = \mathrm{i}\omega\rho c\alpha$, $c$ is the speed of sound in the fluid, and $\mathrm{Re}\,(1 - s^2)$ and $\mathrm{Im}\,(1 - s^2) \geqslant 0$.

The elementary solution $G$ satisfies, by definition, on the plane $z = 0$, the relation

$$\partial G(M, Q)/\partial n_M = \rho\omega^2\alpha G(M, Q), \quad M \in L. \tag{4}$$

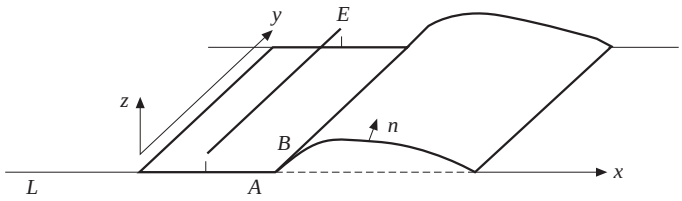


Figure 1. Geometry of the problem: $A$ (on the ground) and $B$ (above the ground) are discretized.

Therefore equation (1) can be decomposed into

$$P(M) = \int_A P(Q)\rho\omega^2(Y(Q) - \alpha)G(M, Q)\,\mathrm{d}S(Q)$$

$$+ \int_B P(Q)[\rho\omega^2 Y(Q)G(M, Q) - \partial G(M, Q)/\partial n_Q]\,\mathrm{d}S(Q) + t(M). \tag{5}$$

When $M$ tends toward the boundaries, particular attention must be taken due to the $\partial G/\partial n_Q$ term. If $M$ is on $A$, equation (5) is still valid, but if $M$ is on $B$ the left side of equation (5) must be multiplied by $\varepsilon(M)$ [12]. $\varepsilon(M)$ is the angle in the medium subtended by the two tangents to the boundary at $M$, divide by $2\pi$. When $M$ is on a smooth part of $S$, $\varepsilon(M) = 1/2$. In this expression, any integral containing a $\partial G/\partial n_Q$ term must be taken in the principal value sense ($PV$) (see the Appendix).

These integral expressions for the pressure on $S$ can be directly used to solve the problem, with a collocation scheme [4]. It consists in using a finite element discretization technique of $S$ into $N$ points and in writing equation (5) at each nodal point. This leads to a set of $N$ linear equations, in terms of the pressures at the $N$ points. The alternative to such a straightforward application of equation (5) is the use of a variational approach. This approach has already been used for acoustical problems [13, 14] or for vibroacoustical situations [15, 16]. Unlike the variational approach described in reference [13], the variational approach described in the next section leads to a symmetric linear system.

## 3. THE VARIATIONAL APPROACH

First one expresses $\partial P/\partial n_M$, when $M$ is on $S$, as

$$(1/\rho\omega^2)(\partial P(M)/\partial n_M) = D(M) + C(M), \tag{6}$$

where

$$D(M) = PV \int_A P(Q)(Y(Q) - \alpha)\frac{\partial G(M, Q)}{\partial n_M}\,\mathrm{d}S(Q) + PV \int_B P(Q)Y(Q)\frac{\partial G(M, Q)}{\partial n_M}\,\mathrm{d}S\,(Q)$$

$$- FP \int_B P(Q)\frac{1}{\rho\omega^2}R(M, Q)\,\mathrm{d}S(Q) + \frac{1}{\rho\omega^2}\frac{\partial t(M)}{\partial n_M}, \tag{7}$$

with

$$R(M, Q) = \partial^2 G(M, Q)/\partial n_M \partial n_Q$$

and

$$C(M) = \begin{Bmatrix} (Y(M) - \alpha)2(1 - \varepsilon(M))P(M) = (Y(M) - \alpha)P(M), & M \in A \\ Y(M)(1 - \varepsilon(M))P(M), & M \in B \end{Bmatrix}. \tag{8}$$

$C(M)$ is obtained, when $M$ tends towards $Q$ on either $A$ or $B$, as a limit contribution of $\partial G(M, Q)/\partial n_M$. The $1 - \varepsilon(M)$ factor is the result of an integration over an infinitely small circular contour around $Q$ on the surface. When $M$ is on $A$, the Green function contributes twice due to the image term. $FP$ denotes the finite part of the integral which is divergent.

The principal value $PV$ is applied either on the $A$ or on the $B$ integral, depending on whether $M$ is on $A$ or $B$. Since either on $A$ or $B$, by definition of $Y$,

$$(1/\rho\omega^2)\partial P(M)/\partial n_M = Y(M)P(M), \tag{9}$$

equation (6) with equations (8) and (9) leads to

$$\alpha P(M) = D(M), \qquad M \in A; \qquad Y(M)\varepsilon(M)P(M) = D(M), \qquad M \in B. \tag{10, 11}$$

The functional is then built by taking successively the two expressions of equation (5) written for $M$ on $A$, then on $B$, and the two equations (10) and (11) obtained from the expression for the normal derivative of the pressure on $A$ and then on $B$. Each of these four integral expressions is multiplied by a test function $q$ associated to $P$ and integrated on $A$ or $B$ with respect to $M$. A more detailed calculation is given in the Appendix. Summing these four double integrals leads to the functional

$$K(q, P) = T(q), \tag{12}$$

where

$$\begin{aligned} K(q, P) = & \iint_{A \times A} Z_{11}(M, Q)P(Q)\,q(M)\,\mathrm{d}S(Q)\,\mathrm{d}S(M) \\ & + \iint_{A \times B} Z_{12}(M, Q)P(Q)q(M)\,\mathrm{d}S(Q)\,\mathrm{d}S(M) \\ & + \iint_{B \times A} Z_{21}(M, Q)P(Q)q(M)\,\mathrm{d}S(Q)\,\mathrm{dS(M)} \\ & + \iint_{B \times B} Z_{22}(M, Q)P(Q)q(M)\,\mathrm{d}S(Q)\,\mathrm{d}S(M) \\ & + \int_{A} (Y(M) - \alpha)P(M)q(M)\,\mathrm{d}S(M), \end{aligned} \tag{13}$$

$$Z_{11}(M, Q) = -\rho\omega^2(Y(M) - \alpha)(Y(Q) - \alpha)G(M, Q),$$

$$\begin{aligned} Z_{22}(M, Q) = & -\rho\omega^2 Y(M)Y(Q)G(M, Q) + Y(M)\partial G(M, Q)/\partial n_Q \\ & + Y(Q)\partial G(M, Q)/\partial n_M - R(M, Q)/\rho\omega^2, \end{aligned}$$

$$Z_{12}(M, Q) = (Y(M) - \alpha)[\partial G(M, Q)/\partial n_Q - \rho\omega^2 Y(Q)G(M, Q)], \qquad M \in A, \qquad Q \in B,$$

$$Z_{21}(M, Q) = (Y(Q) - \alpha)[\partial G(M, Q)/\partial n_M - \rho\omega^2 Y(M)G(M, Q)], \qquad M \in B, \qquad Q \in A,$$

$$T(q) = \int_S q(M)\left[ Y(M)t(M) - \frac{1}{\rho\omega^2}\frac{\partial t(M)}{\partial n_M} \right] \mathrm{d}S(M).$$

The bilinear form $K$ is symmetric since points $M$ and $Q$ may be interchanged. Therefore $K(q, P) = K(P, q)$ and the solution $P$ of the problem is the stationary point of

$$F(P) = \tfrac{1}{2}K(P, P) - T(P). \tag{14}$$

In the previous expressions, the second integration takes care of the local values of $\varepsilon(M)$ not equal to 1/2. The double integrations are all convergent, most especially the integrals containing the double derivative $R$. The finite part of equation (7) due to $R$ is suppressed by the second integration.

The double integration with the $R$ function can be expressed [17] in a different form more convenient for numerical computation. If one recalls that $G$ is the sum of two Hankel functions plus a term $P_\alpha$ for the ground effect, the double derivative of each Hankel function is transformed as

$$\iint \frac{\partial^2 \mathrm{H}_0(M, Q)}{\partial n_M \partial n_Q} P(M)P(Q)\,\mathrm{d}S(Q)\,\mathrm{d}S(M) = \iint [k^2 P(M)P(Q)(\mathbf{n}_M, \mathbf{n}_Q) - (\mathbf{n}_Q \wedge \nabla_Q P(Q),$$

$$\mathbf{n}_M \wedge \nabla_M P(M))]\mathrm{H}_0(M, Q)\,\mathrm{d}S(Q)\,\mathrm{d}S(M), \tag{15}$$

where $\mathbf{n} \wedge \nabla P$ can be written as $\mathrm{d}P/\,\mathrm{d}s$, $s$ being in the tangent direction to the surface [17]. The single and double derivatives of $P_\alpha$ are expressed as

$$\partial/\partial n_M = (\mathbf{n}_M, \nabla_M), \qquad \partial^2/\partial n_M \partial n_Q = (\mathbf{n}_M, \nabla_M(\mathbf{n}_Q, \nabla_Q)). \tag{16}$$

Note that the transformation (15) cannot be applied to $P_\alpha$ since the equality $\nabla_M \mathrm{H}_0 = -\nabla_Q \mathrm{H}_0$ is not satisfied by $P_\alpha$.

## 4. NUMERICAL IMPLEMENTATION

A finite element technique is used to discretize equation (14). Simple linear elements were judged sufficient to discretize the contour $S$. Each double integral is written as a double sum over the $Ne$ elements:

$$\sum_{i=1}^{Ne} \sum_{j=1}^{Ne} \langle \mathbf{P}_i \rangle [\mathbf{Z}_{ij}] \{\mathbf{P}_j\}. \tag{17}$$

$\langle\,\rangle$ and $\{\}$ are respectively line and column vectors.

The elementary matrices $[\mathbf{Z}_{ij}]$ are computed with a classical Gauss double summation. Values of three Gauss points were found to be sufficient. When $i = j$ in equation (17) the elementary integration cannot be done with a simple Gauss technique since it contains a singular part due to the identity of $Q$ and $M$. The singularity $2\pi \log (kr)$ is subtracted from the Green function and the integration is done normally. The singular part is integrated analytically. The computation of the ground function $P_\alpha$ and of its derivative is done by integrating equation (3) with simple Gauss–Laguerre summations as described in reference [4]. Five points per integral were found to give enough precision in most cases.

The Hankel functions may be efficiently evaluated numerically but the time needed is a significant part of the total time of construction of the matrix system. Storing 10 000 values for arguments between 0·001 and 200 and using interpolation whenever the argument falls within this range has allowed reduction of computation times by more than twenty for rigid ground without any reduction of precision.

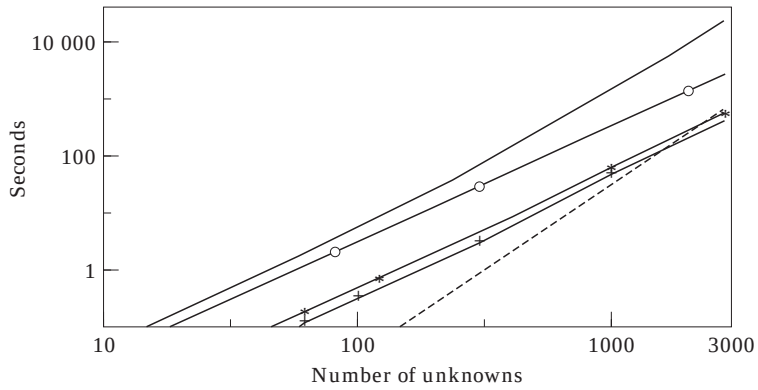


Figure 2. Comparions of the computation times. ——, $P_1$ matrix: rigid ground and screen ($H_0$ computed); +—+, $P_2$ matrix: as $P_1$, $H_0$ tabulated; ∗—∗, $P_3$ matrix: absorbent screen; ○—○, $P_4$ matrix: absorbent ground and screen; - - - - -, $P_5$ resolution time.

Significant reduction of time can be obtained by decomposing the matrix in the form: $\omega^2 A(f_0) + B(f_0) + C(f_0)/\omega^2$. The $A$, $B$, $C$ terms are computed only once, for a central frequency $f_0$ in a given frequency band. This remains valid as long as the main variations come from the $\omega^2$ terms.

Adaptive meshing is easily implemented for 2D contours and also gives very significant reduction of computation times. The contour is defined as a succession of straight elements or portions of circles. At each frequency, every segment is regularly subdivided into a given number of elements per wavelength with a minimum number of elements imposed. Usually values of three up to five elements per wavelength were found sufficient. The matrix system is symmetric and it also contributes to reduce further the computation times. The cumulative effect of these reductions of time in addition to the study of 2D problems with the BEM technique, is that full size problems involving not only a screen but also the profile of a train with its ballast is rendered possible.

The introduction of the effect of the ground in the Green function implies that, when using equation (1), the computation time will be independent of the receiver position. The computer program has been named MICADO which stands in French for Integral Method for the Acoustical Computation of the Diffraction by Obstacles.

In order to provide an idea of the computation times, Figure 2 shows the times needed on a HP 9000 C160 computer, as a function of the number of unknowns $N$. On this

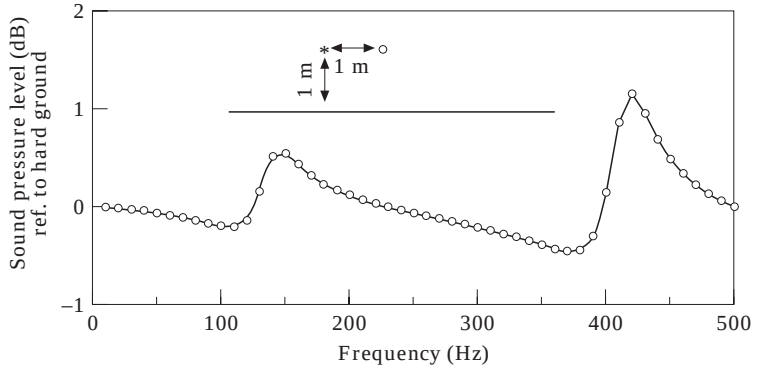


Figure 3. Effect of ground admittance ($\sigma = 300\ \mathrm{kNsm^{-4}}$). ——, MICADO; ○, ground function.

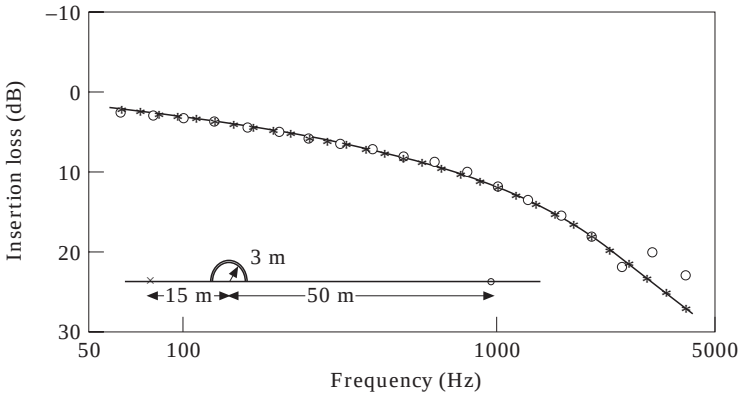


Figure 4. Absorbent barrier of semi-circular section ($\sigma = 300$ kNsm$^{-4}$). ——, Analytical; *, MICADO; ○, Hothersall *et al*.

computer 1600 million multiplications can be performed in one second. Five different plots are given. $P_1$ to $P_4$ represent the times necessary to compute the matrix and $P_5$ is the resolution time. $P_1$ and $P_2$ were obtained for a rigid problem either by computing or by using the tabulated values of the Hankel functions. $P_3$ corresponds to a fully absorbent screen with rigid ground, whereas in $P_4$ the ground becomes also absorbent. The time needed to compute the matrices varies as the square of $N$ and the time to solve the matrix system varies as the third power of $N$. For very large discretization the total time may therefore increase rapidly with frequency, but in practice this is seldom the case.

At 2000 Hz, the total time for a straight screen, 3 m high, meshed with three elements per wavelength and one observation point is 0·8 s. It becomes 6·5 s if the ground is absorbent. Adding the train profile of Figure 7 leads to 12 s if the ground is rigid and 69 s for an absorbent ground.

## 5. SIMPLE CASES

The simple case of a source over an infinite ground of constant admittance is first considered. The source and the receiving points ($E$, $M$) are 1 m apart, both 1 m above ground. The admittance corresponds to a flow resistivity $\sigma$ of 300 kNsm$^{-4}$ in the Delany

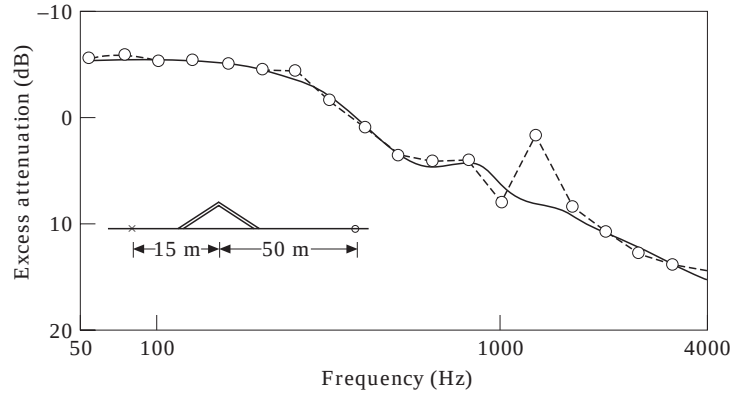


Figure 5. Pyramidal barrier, 3 m high, 12 m wide. ——, MICADO; ○ - - - ○, Hothersall *et al*.

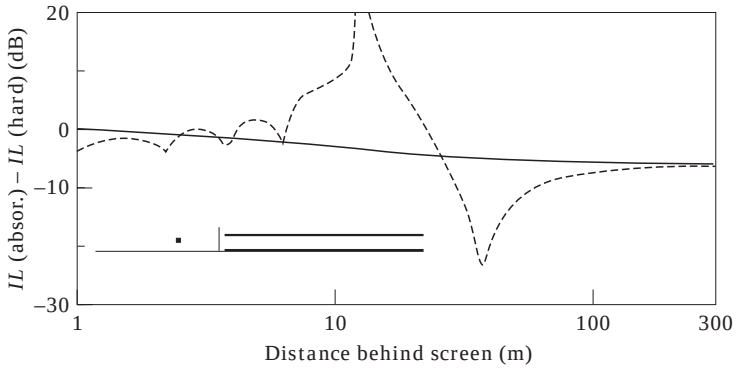


Figure 6. Long distance effect of ground admittance ($\sigma = 300$ kNsm$^{-4}$); insertion loss ($IL$) relative to $IL$ for hard ground at 500 Hz. ——, 0·1 m above ground; - - - -, 2 m above ground.

and Bazley model [18]. Figure 3 gives the level difference of pressure at $M$ for absorbent and hard grounds. The soft ground is modelled either by meshing the ground 40 m around $E$, the rest of the floor being hard, or by using equations (2) and (3). The results are identical, which validates the BEM program especially for elements on the ground.

Comparisons with results obtained in reference [9] with a collocation method are presented in Figures 4 and 5. In Figure 4, the case of a barrier of semi-circular section and radius 3 m is considered. The ground is hard and the barrier has an admittance given by $\sigma = 300$ kNsm$^{-4}$. The excess attenuation (free field pressure divided by pressure with screen) is obtained for both source and receiver on the ground, so that no interference effect is present. This problem has an analytical solution which has been given in reference [19]. The solution obtained with MICADO agrees perfectly with the exact solution whereas the collocation solution shows errors at high frequencies. In Figure 5, a screen of triangular shape with the same admittance is presented. Again some differences between MICADO and the collocation solution of equation [9] can be seen. The occurrence of the so-called "irregular frequencies", corresponding to the resonance frequencies of the complementary interior problem, is at the origin of the instabilities obtained with the collocation approach. At such frequencies there is not a unique numerical solution of the problem [9]. The variational approach, presented in this paper, does not seem to have this problem and this has been checked numerically. Only poor meshing may lead to numerical imprecisions at these frequencies. Using five elements per wavelength has been found sufficient to avoid the problem in most cases.

Ground effect on long distance propagation is illustrated in Figure 6 by plotting the difference of insertion loss (pressure without screen divided by pressure with screen) for absorbent and hard ground ($\sigma = 300$ kNsm$^{-4}$) behind a hard flat screen, 3·0 m high, for

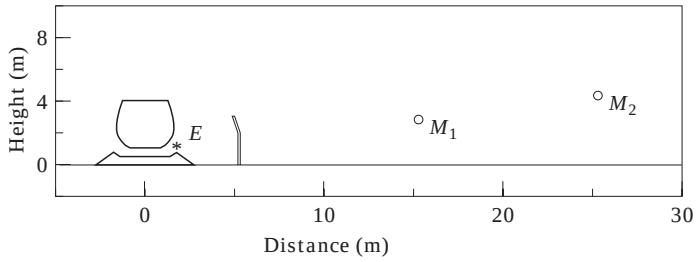


Figure 7. General view of screen, train, ballast, source $E$ and two receiver positions $M_1$, $M_2$.

a receiver at $z = 0{\cdot}1$ of 2 m above the ground, at 500 Hz. The source is at $z = 1{\cdot}5$ m and 5 m in front of the screen. At 300 m, the insertion loss would be overestimated by 7 dB if the absorption of the ground were not taken into account.

## 6. SCREENS NEAR TRAINS

Consider now the configuration of Figure 7, with the 2D section of a train on a ballast, with a 3·05 m high screen placed 5·25 m away from the center of the train. $E$ is a line source close to the train, at position (1·5, 1·25). Two receiving points $M_1$ and $M_2$ are considered at (15·25, 2·75) and (25·25, 4·25). The train is rigid. The ballast has an admittance corresponding to $\sigma = 100$ kNsm$^{-4}$ which is a simplified way of describing its behaviour.

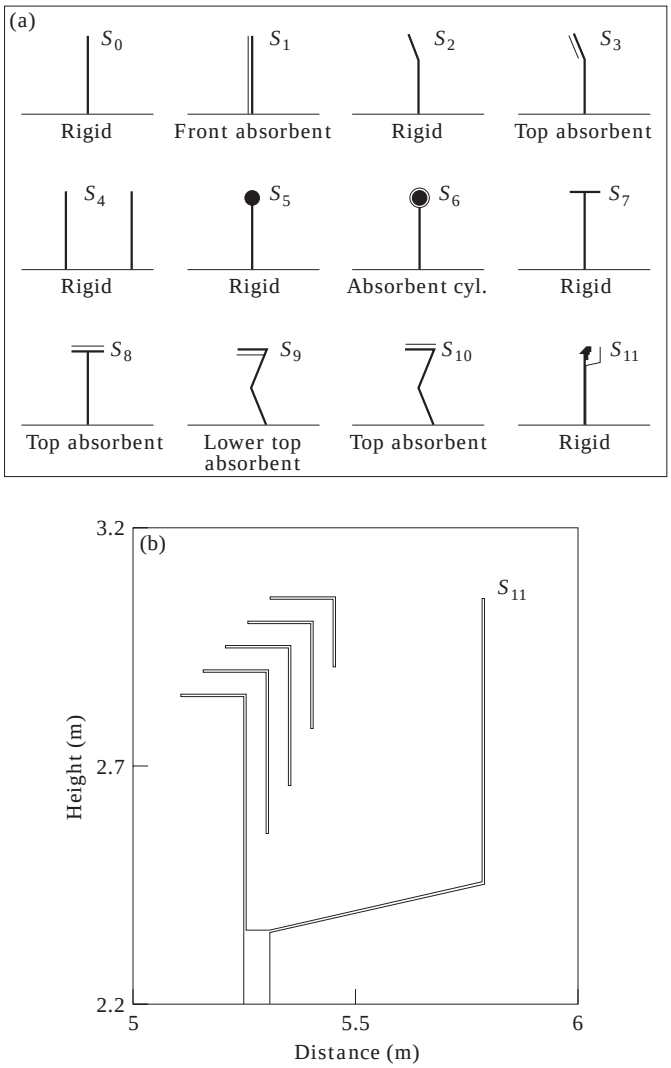


Figure 8. (a) Different screens, 3·05 m high; $S_2$, $S_3$ are tilted by 26°, 1·97 m above ground; the two screens of $S_4$ are 3 m apart; the cylinders in $S_5$ and $S_6$ have a diameter of 0·5 m; $S_7$, $S_8$, $S_9$ have a 1 m wide top; $S_8$, $S_9$ have a 0·5 m wide inflection at mid-height; (b) top view of $S_{11}$ ("calm zone" device) with co-ordinates according to Figure 7.

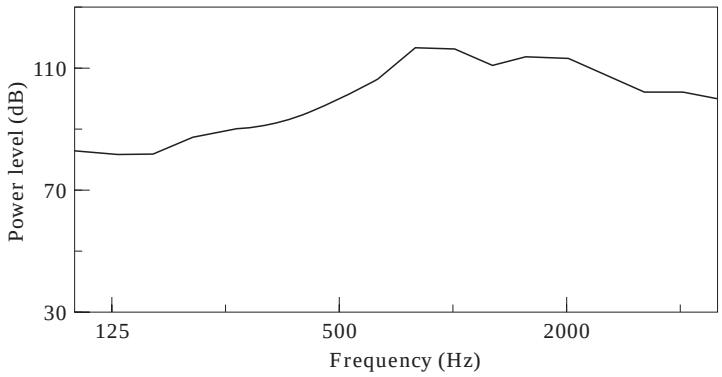


Figure 9. Power level of line source.

The absorptive coatings on the screens have a flow resistivity of $\sigma = 30\,\mathrm{kNsm}^{-4}$ and a thickness of 5 cm, corresponding to a mineral wool. Several screens are considered and described in Figure 8. They all have the same total height of 3·05 m,, which is important for comparison purposes. $S_0$ denotes the case of the straight screen without treatment, and it will be the reference situation. $S_2$ and $S_3$ are tilted towards the source. $S_4$ is made of two identical hard screens. $S_5$ and $S_6$ have a cylinder on top (diameter 0·5 m), hard in $S_5$ and absorbent in $S_6$, $S_7$ and $S_8$ are $T$ screens either hard or treated on the top. $S_9$ and $S_{10}$ are sigma shaped screens with treatment either on the underside of on the upperside of the top. $S_{11}$ is a ≪calm zone≫ type of screen [21]. The computations were done with twenty frequencies per third-octave band. This was found necessary for convergence. Figure 9 shows the sound power of source $E$.

In Figure 10, the insertion losses of screens $S_0$, $S_1$, $S_8$ and $S_{10}$ (rigid and treated straight screens, $T$ and sigma screens treated on the top) at point $M_2$, with the screen present and the train absent are plotted. The ground is hard. $S_0$ and $S_1$ have very similar insertion losses meaning that the treatment of the front side with a mineral wool is of small effect. $S_8$ and $S_{10}$ also have similar losses, meaning that a $T$ and a sigma screen of the same overall dimensions and the same treatment on the top have similar effects without the train. These remarks are no longer valid when the train and ballast are introduced, as it can be seen

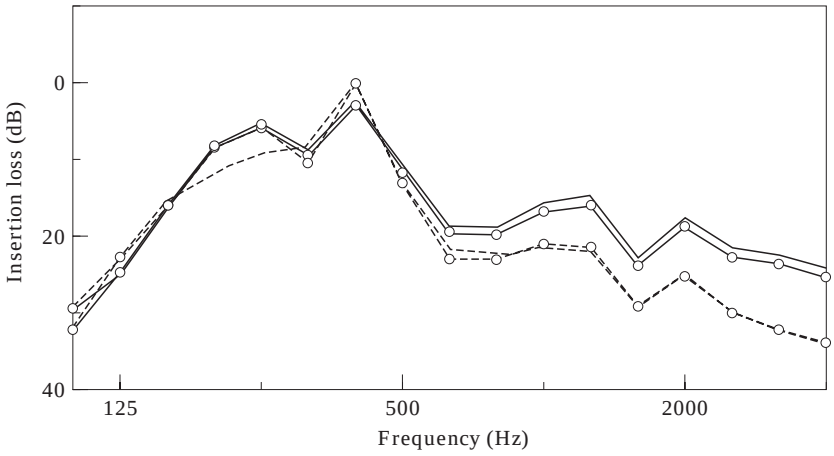


Figure 10. Different screens, without train. ——, $S_0$; ○——○, $S_1$; - - - -, $S_8$; ○ - - - - ○, $S_{10}$.

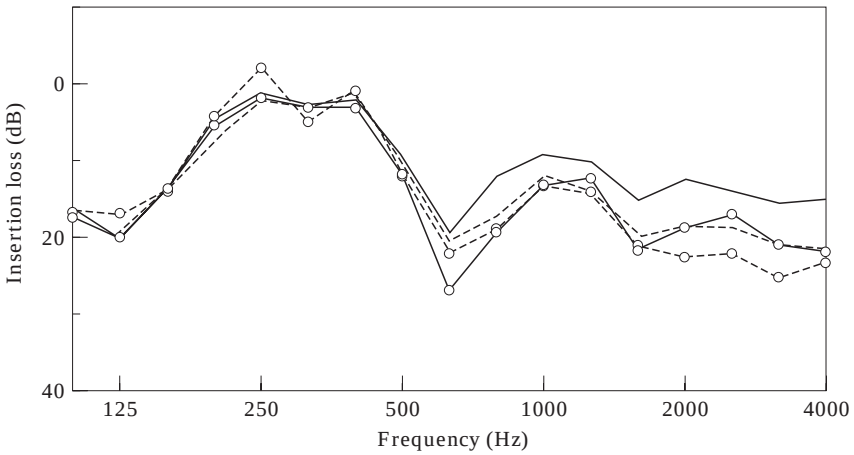


Figure 11. Different screens, with train. Key as for Figure 10.

in Figure 11. In this case treating the straight screen improves its efficiency significantly since it reduces the standing waves between car and screen. Moreover, the sigma shape further improves the $T$ screen above 500 Hz, due also to the modification of the standing wave pattern. It can therefore be concluded from these results, that comparing screens placed near trains should not be done without modelling the profile of the train.

The values of attenuation terms of the A-weighted level (dB(A)), relative to the case of a single hard screen, are listed in Table 1. Results at points $M_1$ and $M_2$ are reported for hard or absorbent ground ($\sigma = 600$ kNsm$^{-4}$) either with or without the train. The values in parenthesis are for the point $M_2$. The dB(A) values are obtained for the source spectrum of Figure 9. This table shows the following: without the car, the absorbing material placed on the vertical screen ($S_1$) has little effect but with the car its efficiency is in the order of 4 or 5 dB(A); tilting the top ($S_2$) has little effect, adding some absorption ($S_3$) improves the result; adding a second screen ($S_4$) is efficient for points in the shadow zone; a rigid

TABLE 1

*Gains in* dB(A) *of different screens relative to the straight screen* ($S_0$); *ground is either hard or absorbent* ($\sigma = 600\ kNsm^{-4}$); *two receiving points* $M_1$ *and* ($M_2$) *either with or without the train + ballast*. (*Screens* $S_0$ *to* $S_{11}$ *defined in Figure* 8)

| | No train | | With train | |
|---|---|---|---|---|
| Ground | Hard | Absorbent | Hard | Absorbent |
| $S_1$ | 1·2 (1·0) | 1·1 (0·9) | 4·7 (5·2) | 3·6 (3·9) |
| $S_2$ | 2·3 (0·0) | 1·7 (0) | 0·7 (1·1) | 1·0 (1·4) |
| $S_3$ | 3·0 (0·7) | 2·4 (0·6) | 2·7 (2·8) | 3·2 (4·5) |
| $S_4$ | 7·0 (3·0) | 6·7 (2·8) | 4·5 (1·6) | 4·6 (1·7) |
| $S_5$ | −1·4 (−1·9) | −3·7 (−5·2) | −2·8 (−2·0) | −3·1 (−2·3) |
| $S_6$ | 3·6 (2·8) | 3·2 (2·4) | 2·4 (1·8) | 2·1 (1·4) |
| $S_7$ | 2·3 (0·6) | 1·8 (0·2) | 1·8 (1·0) | 1·5 (0·6) |
| $S_8$ | 6·8 (5·0) | 6·3 (4·6) | 5·5 (4·0) | 5·2 (3·5) |
| $S_9$ | 2·6 (0·9) | 2·1 (0·5) | 4·5 (3·8) | 3·9 (2·8) |
| $S_{10}$ | 7·0 (5·1) | 6·3 (4·6) | 7·0 (5·4) | 6·7 (4·8) |
| $S_{11}$ | 5·1 (3·7) | 4·6 (3·3) | 1·9 (1·2) | 1·7 (0·9) |

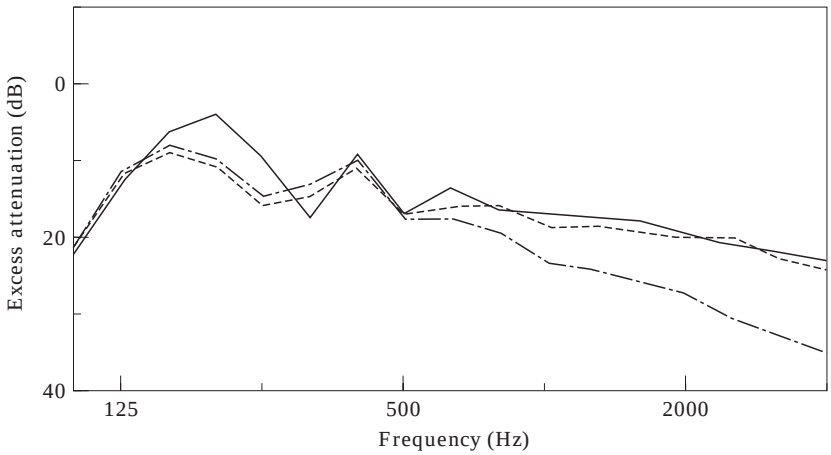


Figure 12. Excess attenuation at $M_1$ (15, 3); coherent line source; ground ($\sigma = 300\,\mathrm{kNsm^{-4}}$); three screens. ——, Straight; - - - -, rigid T; — - —, T with lining on top.

cylinder ($S_5$) placed on the top of a screen degrades its efficiency whereas an absorbent cylinder ($S_6$) gives an improvement of the order of 1 to 2 dB(A); the T-shaped screen if hard ($S_7$) improves the straight screen by 1 or 2 dB(A), and by more than 4 dB(A) if treated at the top ($S_8$); the sigma shaped screen should be treated at its top ($S_{10}$) and gives similar results as a T screen of same overall dimensions if the train is not considered, but introducing the train leads to even better results due to the broken shape of the screen and putting treatment on the front side would further improve these results; the ⟪calm zone⟫ system ($S_{11}$) gives improvements of the order of only 1 or 2 dB(A).

## 7. INFLUENCE OF SOURCE TYPE

It is interesting to see the influence of the type of source used in the model. The 2D problem implies that the source is an infinite coherent line source. Recent works by Duhamel [11] have shown that post-treating the 2D results via a Fourier type of transform,

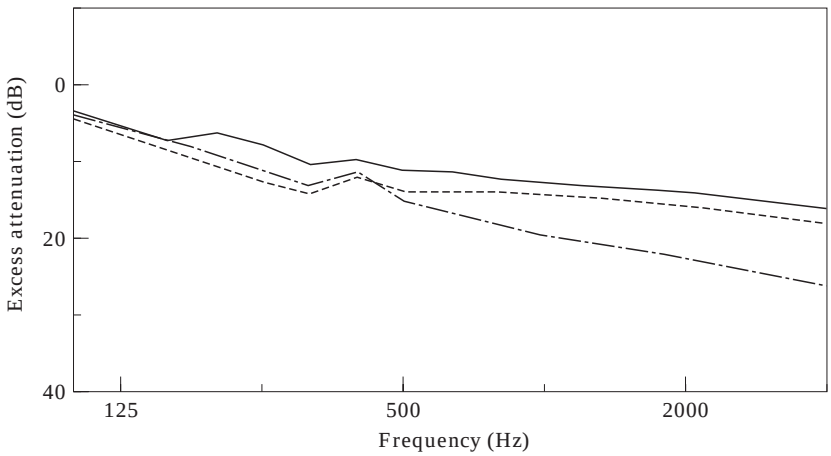


Figure 13. Excess attenuation at $M_1$ (15, 3); incoherent line source; ground ($\sigma = 300\,\mathrm{kNsm^{-4}}$). Key as for Figure 12.

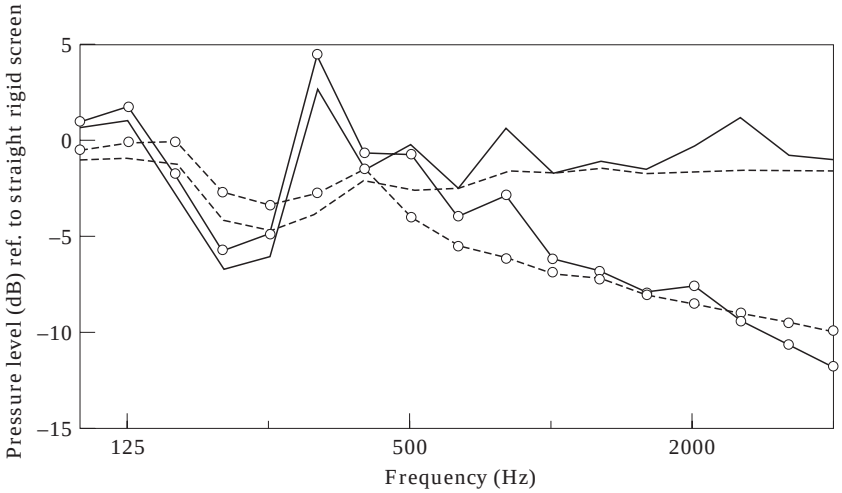


Figure 14. Effect of T top at $M_1$ (15, 3); coherent ($C$) or incoherent ($I$) source; rigid ($R$) or absorbent ($A$) T top; ($\sigma = 30$ kNsm$^{-4}$). ——, $C$ ($R$); ○——○, $C$ ($A$); - - - - , $I$ ($R$); ○ - - - ○, $I$ ($A$).

gives the solution for a still infinite geometry but for either a point source, a combination of point sources at any 3D points or for an infinite incoherent line source. The 2D problem must be solved for real frequencies up to the 3D frequency of interest as well as for some imaginary frequencies. When ground and obstacles are rigid, the same 2D spectrum serves for all the 3D frequencies below the highest 2D frequency computed. When absorbent surfaces are present (ground or obstacle), the 2D solution must be obtained for every 3D frequency with a modified admittance spectrum. This extra-cost is negligible compared to the time that full 3D computations would involve [11].

Figure 12 shows the excess attenuation of the straight rigid screen ($S_0$), the rigid T screen and the same T screen with mineral wool on the top (cases $S_7$ and $S_8$) in the case of a coherent line source. The receiver is at (15, 3) and the ground has an impedance given by $\sigma = 300$ kNsm$^{-4}$. Figure 13 shows the same results for the incoherent line source, after using the 3D transformation. In the second case, the attenuations are more regular and of smaller amplitude at high frequencies than for the coherent source. Figure 13 was obtained with one frequency per third octave band and due to the regularity of the curves

TABLE 2

*Excess attenuation in* dB(A); *three types of screens* 2 *points* $M_3$(15, 3), $M_4$(100, 4); ($C$, $I$) *coherent or incoherent line sources*; ($R$, $A$) *rigid or absobent ground*; *values in parentheses are relative to the straight screen*

| | | | Straight | T screen | T treated |
|---|---|---|---|---|---|
| R | C | $M_3$ | 16·8 | 17·9 (1·1) | 22·4 (5·6) |
| | | $M_4$ | 16·5 | 17·4 (0·9) | 22·1 (5·6) |
| | I | $M_3$ | 9·3 | 10·6 (1·3) | 17·3 (8·0) |
| | | $M_4$ | 8·6 | 9·7 (1·1) | 15·4 (6·8) |
| A | C | $M_3$ | 17·5 | 18·2 (0·7) | 22·7 (5·2) |
| | | $M_4$ | 16·4 | 17·1 (0·7) | 21·1 (4·7) |
| | I | $M_3$ | 13·1 | 14·8 (1·7) | 20·2 (7·1) |
| | | $M_4$ | 14·7 | 15·5 (0·8) | 20·1 (5·4) |

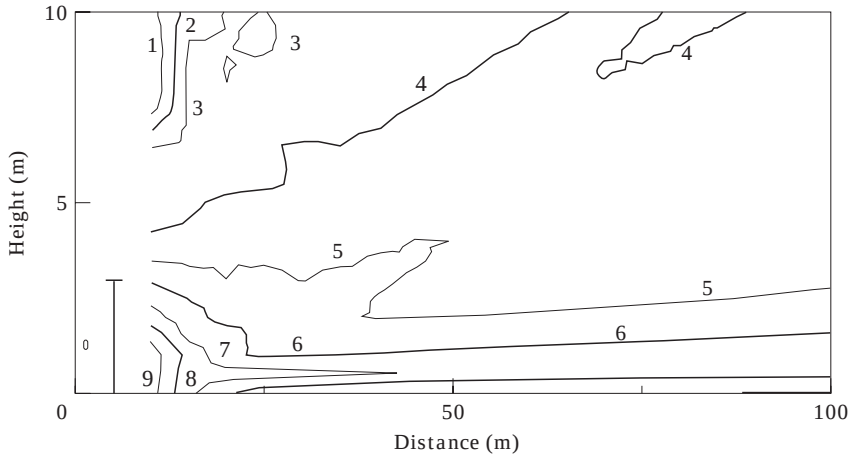


Figure 15. Efficiency in dB(A) of a T screen, top absorbent ($\sigma = 30$ kNsm$^{-4}$) referred to a straight hard screen; thick lines are even values; absorbent ground ($\sigma = 300$ kNsm$^{-4}$); coherent line source.

it seems sufficient. Results for the coherent line source were obtained with twenty frequencies per third octave band.

Figure 14 compares at $M_3$ (15, 3), the pressure levels for both T screens relative to the straight screen and for either coherent (solid curve) or incoherent line sources (dashed curves). Both types of sources give similar overall results. Again, the incoherent line source gives much smoother results.

The excess attenuation values in dB(A) for the three types of screens and the two types of sources, at point $M_3$ and $M_4$ (100, 4) are given in Table 2, both for rigid and absorbent ground. Smaller attenuations are obtained for incoherent than for coherent line sources, the difference being higher at $M_3$, the point closer to the screen. Differences between incoherent and coherent line sources are smaller with an absorbent ground. The efficiency of an added absorption on the T top is higher for incoherent than for coherent sources (8 versus 5·6 dB(A) at point $M_3$ for a rigid ground, and 7·1 versus 5·2 dB(A) at point $M_3$

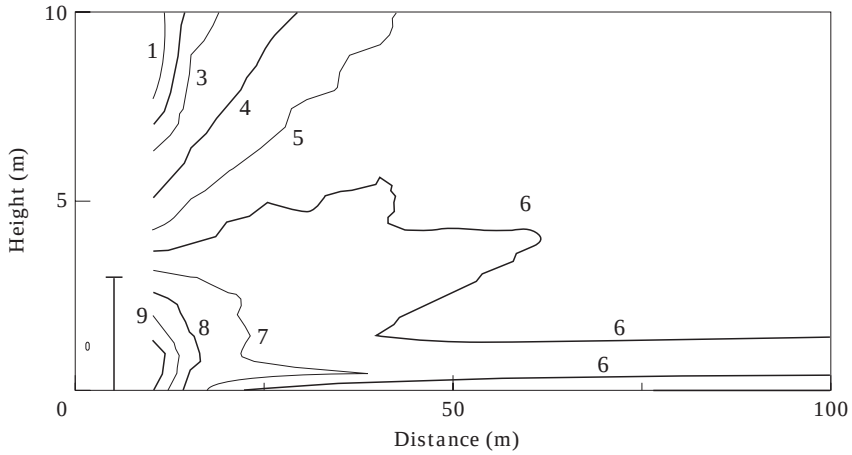


Figure 16. Efficiency in dB(A) of a T screen, top absorbent ($\sigma = 30$ kNsm$^{-4}$) referred to a straight hard screen; thick lines are even values; absorbent ground ($\sigma = 300$ kNsm$^{-4}$); incoherent line source.

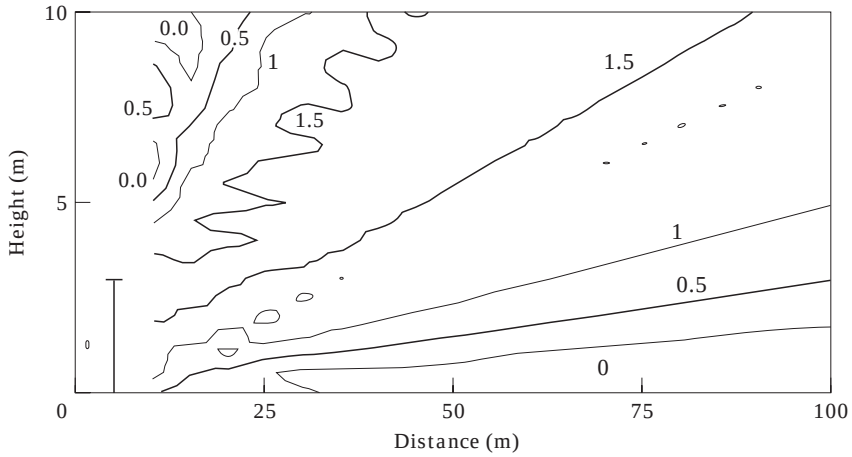


Figure 17. Effect of source type on the efficiency *ET* in dB(A) of the top of a T screen; *ET* incoherent–*ET* coherent; ground ($\sigma = 300\ \mathrm{kNsm^{-4}}$); thin lines are integer values.

for an absorbent ground). In general the treatment of the top of the T screen increases its efficiency by more than 4 dB(A).

Figures 15 and 16 show, in the form of iso-contour plots, the gain in dB(A) on absorbent ground of the T screen with treatment on the top, referenced to the straight hard screen, first for the coherent then for the incoherent line source. Figure 17 shows the difference between Figures 16 and 15, positive values indicating a higher efficiency of the absorbent T top for an incoherent than for a coherent line source. The values are of the same order of magnitude in both cases for the lower points, differences of 1 or 2 dB(A) may be found at the highest positions.

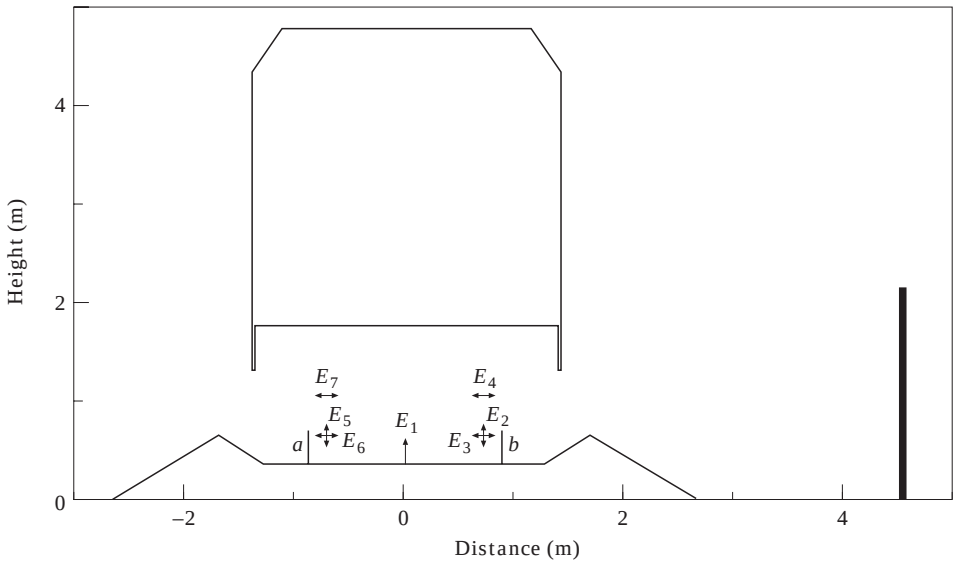


Figure 18. Geometry of train, ballast, screens ($a$, $b$), sources (dipoles 1 to 7) and barrier.

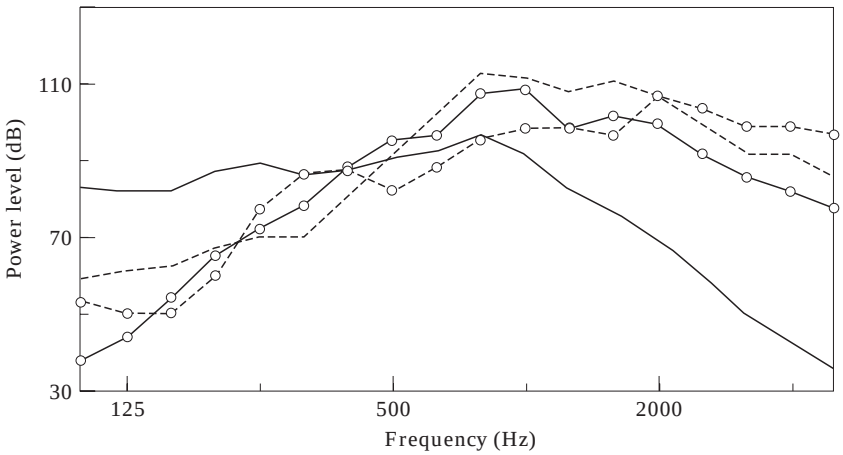


Figure 19. Separate powers of dipole sources. ——, Sleeper $V$; - - - -, rail $V$; ○——○, rail $H$; ○ - - - -○, wheel $H$.

In the case of an incoherent line source, the efficiency of the absorbent top has been found to be about 1 dB(A) lower for the absorbent ground than for the hard ground, at most points.

## 8. EFFECT OF LITTLE SCREENS CLOSE TO THE RAILS

The last case presented concerns the use of little screens placed near the rails. Figure 18 shows a view of the 2D profile of the bodywork of a train above ballast, a vertical straight barrier, 2·15 m high, with mineral wool facing the train ($\sigma = 30\,\mathrm{kNsm^{-4}}$, thickness = 5 cm) and two little screens near the rails. Whereas the train profile of Figure 7 corresponds to a TGV train, this profile is typical of more classical trains. The noise radiated by the lower part of the car is modelled with seven dipoles. Three vertical dipoles for the sleeper ($E_1$), right ($E_2$) and left ($E_5$) rails and four horizontal dipoles for right ($E_3$) and left ($E_6$) rails and right ($E_4$) and left ($E_7$) wheels. Figure 19 gives the separate contributions of these sources, as given by the European Rail Research Institute [5, 6].

The sources are assumed to be totally incoherent. Therefore, each problem is solved seven times and the sound power levels are summed in energy at all points of interest. It should be noted that this does not involve a multiplication of the total computation time by a factor of seven, since the resolution algorithm, based on a Cholevsky decomposition

TABLE 3

*Efficiency in* dB(A) *of small screens placed near the rails*; *three heights of screens*: 55, 105, 155 mm *above rail head*

| | Receivers Position | $M_1$ 25, 5·65 | $M_2$ 25, 10 | $M_3$ 25, 14 | $M_4$ 50, 5·65 | $M_5$ 50, 20 | $M_6$ 50, 26 | $M_7$ 100, 5·65 | $M_8$ 100, 40 | $M_9$ 100, 50 |
|---|---|---|---|---|---|---|---|---|---|---|
| Hard | 55 mm | −0·4 | −0·3 | +0·6 | −0·2 | −0·4 | +0·3 | 0 | −0·4 | +0·1 |
| screens | 105 mm | −0·5 | −0·1 | +1·2 | −0·1 | −0·1 | +0·7 | +0·1 | −0·2 | +0·6 |
| | 155 mm | −0·7 | 0 | +1·5 | −0·1 | 0 | +1·0 | −0·1 | 0 | +0·7 |
| Absorbent | 55 mm | +1·2 | +1·5 | +2·4 | +1·3 | +1·3 | +2·0 | +1·6 | +1·3 | +1·9 |
| screens | 105 mm | +1·8 | +2·3 | +3·6 | +1·9 | +2·1 | +3·0 | +2·3 | +2·1 | +2·8 |
| | 155 mm | +2·3 | +3·0 | +4·7 | +2·6 | +2·8 | +4·0 | +2·8 | +2·9 | +3·7 |

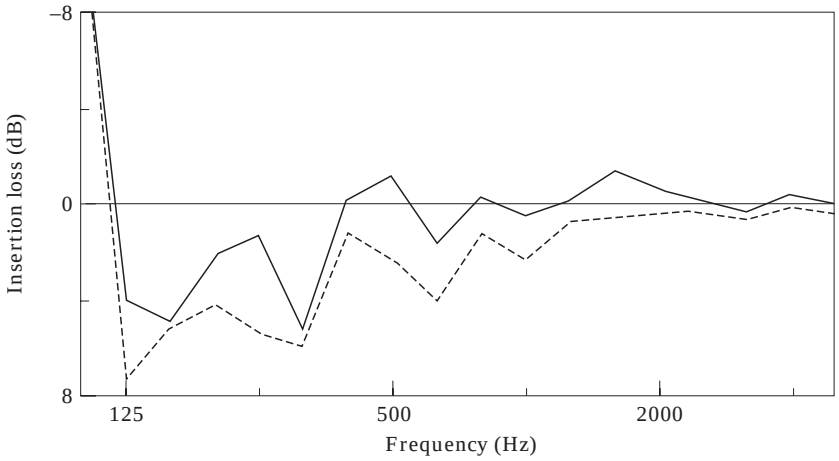


Figure 20. Efficiency of little screens at $M_4$ (50, 5·65). ——, rigid screens; - - - - , absorbent screens.

[20], stores an intermediate decomposition of the matrix once for all and that the back-substitution, different for the various sources, is a minor percentage of the total resolution time. Consequently, dealing with seven sources only adds a few percent of computation time compared to the case with only one source, provided that only a few pressure points are wanted.

Nine receiving points are considered at 20, 45 and 95 m behind the screen and for every distance at three different heights such that one is deep in the shadow zone ($M_1$, $M_4$, $M_7$), one is in the transition zone ($M_2$, $M_5$, $M_8$) and one is in direct view from the sources ($M_3$, $M_6$, $M_9$). The exact positions with respect to Figure 18 are given in Table 3. Figure 20 compares the extra insertion loss due to the little screens at point $M_4$ (45 m behind screen and 5·65 m above ground) when these screens are either hard or covered with the same mineral wool as the barrier. In this case the screens project 55 mm above the rails head. One can notice that hard screens placed near the rails reduce the efficiency of pre-existent barriers. If these screens are absorbent, a significant improvement can be obtained. At 100 Hz, the little screens degrade the results, even if they are treated. Figure 21 shows the sound pressure level, referenced to point (2, 2), for a vertical dipole (source $E_2$, right rail) placed near a little screen. Instead of having a horizontal minimum, the radiation pattern is strongly modified by the presence of the screen and leads to a horizontal maximum. This has been found to be the reason for the overall degradation, when the contributions of the seven sources are added. Finally Table 3 summarizes for the nine receiving positions the efficiency in dB(A) of three heights of screens either hard or treated. These results further enhance the efficiency of putting absorbent little screens near rails since between

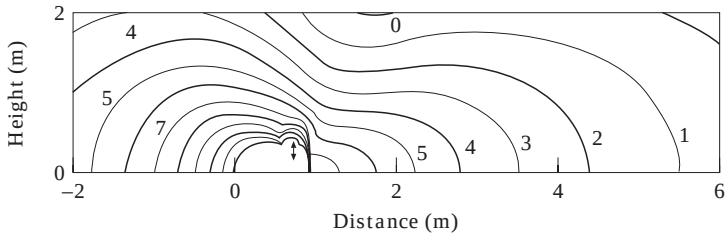


Figure 21. Effect of screen on vertical dipole; source $E_2$ (right rail) at 100 Hz; lines every 1·5 dB.

1 and 4 dB(A) of noise reduction can be expected. Further calculations have shown that 1 or 2 more dB(A) of attenuation can be obtained by placing the same absorbent wool ($\sigma = 30\ \mathrm{kNsm^{-4}}$, thickness = 5 m) under the car.

## 9. CONCLUSIONS

The application of boundary element methods to 2D situations enables the study of complex situations for the full frequency range of interest. A variational approach has been chosen since it leads to a symmetric matrix and provided that sufficient meshing is used, the results are not affected by the problem of irregular frequencies. The introduction of Green functions which include absorbent ground effects, contributes to the rapidity of the computations. Recent works by Duhamel give a way to bypass the major drawback of 2D approaches since they offer a mean of post-treating the 2D results to rapidly obtain solutions for either point sources of incoherent line sources. The geometry remains infinite but this is of minor importance due to the practical length of barriers placed near trains or roads. Applications to railway problems fully show the capacities of the method as well as the necessity of introducing the train profiles for assessing the efficiency of different screens.

## ACKNOWLEDGMENT

The author expresses his gratitude to the European Rail Research Insitute project which funded the railway applications of this work [5, 6].

## REFERENCES

1. Z. Maekawa 1986 *Applied Acoustics* **1**, 157–173. Noise reduction by screens.
2. T. Kawai 1981 *Journal of Sound and Vibration* **79**, 229–242. Sound diffraction by a many-sided barrier or pillar.
3. K. Attenborough 1995 *Journal of the Acoustical Society of America* **97**, 173–191. Benchmark cases for outdoor sound propagation models.
4. S. N. Chandler-Wilde and D. C. Hothersall 1995 *Journal of Sound and Vibration* **180**, 705–724. Efficient calculation of the Green function for acoustic propagation above a homogeneous impedance plane.
5. P. Jean and Y. Gabillet 1994 (March) *ERRI Report WGC6/CT0/7/10.302/0675*. Study of the possibilities of improving existent noise barriers.
6. P. Jean and Y. Gabillet 1996 (November) *ERRI WG6/NST0/7/10.297/022*. Multiple barrier effect.
7. P. Jean and Y. Gabillet 1995 *Euronoise* 95, 251–256. A boundary element method program to study 2D noise barriers with ground effects.
8. Y. Gabillet, P. Jean and J. Defrance 1997 *Internoise* 97. A boundary element formalism for the study of noise barriers.
9. D. C. Hothersall, S. N. Chandler-Wilde and M. N. Hajmirzae 1991 *Journal of Sound and vibration* **146**, 303–322. Efficiency of single noise barriers.
10. D. Duhamel and P. Sergent *Submitted for publication*. Numerical calculation of the three-dimensional sound pressure around noise barriers built over ground of infinite impedance.
11. D. Duhamel 1996 *Journal of Sound and Vibration* **197**, 547–571. Efficient calculation of the three-dimensional sound pressure field around a noise barrier.
12. R. D. Ciskowski and C. A. Brebbia 1991 *Computational Mechanics Publications Elsevier Applied Science*: *Boundary Element Methods in Acoustics*. Amsterdam: Elsevier.
13. R. Seznec 1980 *Journal of Sound and Vibration* **73**, 195–209. Diffraction of sound around barriers: use of the boundary elements technique.
14. M. A. Hamdi 1982 *Thèse de doctorat d'état*, *Université de Technologie de Compiègne*.

Formulation variationnelle par équations intégrales pour le calcul de champs acoustiques linéaires proches et lointains.
15. P. JEAN 1985 *Thèse de doctorat*, *Université de Technologie de Compiègne*. Une méthode variationelle par équations intégrales pour la résolution numérique de problèmes intérieurs et extérieurs de couplage élasto-acoustique.
16. P. JEAN and M. A. HAMDI 1985 *Colloque Tendances actuelles en calcul des structures*. *Bastia*, 6–8 *Novembre*. Résolution numérique des problèmes couplés par une méthode d'éléments finis de frontière.
17. C. MONKALA 1988 *Thèse de doctorat*, *Université de Technologie de Compiègne*. Effet des singularités géométriques sur les résultats numériques d'une méthode d'éléments finis de frontière dans un problème plan.
18. M. E. DELANY and E. N. BAZLEY 1970 *Applied Acoustics* **3**, 105–116. Acoustical properties of fibrous absorbent materials.
19. J. E. COLE, III 1987 *Journal of the Acoustical Society of America* **81**, 222–225. Diffraction of sound by a refracting cylindrical barrier.
20. W. H. PRESS, S. A. TEUKOLSKY, W. T. WETTERING and B. P. FLANNERY 1994 *Numerical recipes*. Cambridge University Press.
21. G. R. WATTS and P. A. MORGAN 1996 *Applied Acoustics* **49**, 1–16. Acoustic performance of an interference-type noise-barrier profile.

## APPENDIX: COMPUTATION OF THE FUNCTIONAL

The expressions for the pressure and its derivative when the point $M$ is either on $A$ or on $B$ are written for a smooth point, where $\varepsilon(M) = 1/2$. The influence of angular positions is cancelled by the second integration.

When $M \in A$, the pressure can be written as

$$P(M) - \int_A P(Q)\rho\omega^2(Y(Q) - \alpha)G(M\,Q)\,\mathrm{d}S(Q)$$

$$- \int_B P(Q)\left[\rho\omega^2 Y(Q)G(M, Q) - \frac{\partial G(M, Q)}{\partial n_Q}\right]\mathrm{d}S(Q) = t(M). \tag{A1}$$

If $M \in B$,

$$\frac{P(M)}{2} - \int_A P(Q)\rho\omega^2(Y(Q) - \alpha)G(M\,Q)\,\mathrm{d}S(Q)$$

$$- \int_B P(Q)\left[\rho\omega^2 Y(Q)G(M, Q) - \frac{\partial G(M, Q)}{\partial n_Q}\right]\mathrm{d}S(Q) = t(M). \tag{A2}$$

If $M \in A$, equations (10), (7) and (4) lead to

$$\int_A P(Q)(Y(Q) - \alpha)\rho\omega^2\alpha G(M, Q)\,\mathrm{d}S(Q) + \int_B P(Q)\,Y(Q)\rho\omega^2\alpha G(M, Q)\,\mathrm{d}S(Q)$$

$$- \int_B P(Q)\alpha\frac{\partial G(M, Q)}{\partial n_Q}\,\mathrm{d}S(Q) - \alpha P(M) = -\frac{1}{\rho\omega^2}\frac{\partial t(M)}{\partial n_M}. \tag{A3}$$

When $M \in B$, equation (11) can be written as

$$\int_A P(Q)(Y(Q) - \alpha) \frac{\partial G(M, Q)}{\partial n_M} \, \mathrm{d}S(Q) + PV \int_B P(Q) Y(Q) \frac{\partial G(M, Q)}{\partial n_M} \, \mathrm{d}S(Q)$$

$$- FP \int_B P(Q) \frac{1}{\rho \omega^2} R(M, Q) \, \mathrm{d}S(Q) - \frac{Y(M)}{2} P(M) = -\frac{1}{\rho \omega^2} \frac{\partial t(M)}{\partial n_M} . \quad \text{(A4)}$$

The functional is then directly derived by computing

$$\int_A (A1) q(M) Y(M) \, \mathrm{d}S(M) + \int_A (A3) q(M) \, \mathrm{d}S(M)$$

$$+ \int_B (A2) q(M) Y(M) \, \mathrm{d}S(M) + \int_B (A4) q(M) \, \mathrm{dS}(M), \quad \text{(A5)}$$

where $q$ is a test function.